Efficiency of a compact CO_2 coaxial plasma torch driven by ultrafast microwave power pulsing: stability and plasma gas flow dynamics

S.Soldatov[1], E. Carbone[2], A. Kuhn[3], G. Link[1], J. Jelonnek[1], R. Dittmeyer[3], A. Navarrete[3]

[1.] Institute for Pulsed Power and Microwave Technology (IHM), Karlsruhe Institute of Technology (KIT), Hermann-von-Helmholtz-Platz 1, 76344 Eggenstein-Leopoldshafen, Germany

[2.] Institut National de la Recherche Scientifique, centre Énergie Matériaux Télécommunications, 1650 blvd Lionel Boulet, J3X 1P7 Varennes, QC, Canada

[3.] Institute for Micro Process Engineering (IMVT), Karlsruhe Institute of Technology (KIT), Hermann-von-Helmholtz-Platz 1, 76344 Eggenstein-Leopoldshafen, Germany

Abstract. Ultrafast pulsation of microwave power for CO_2 conversion using plasmas is a mean to improve the efficiency of the process. Nevertheless, the fundamental phenomena involved need deeper understanding in order to design optimal plasma based devices. Therefore, detailed parametric scans of the plasma torch performance are performed with plasma diagnostics to unravel the underlying mechanisms limiting the CO yield. Very short pulsed plasmas have low CO_2 conversion because of the energy cost needed to generate the plasma itself. For power pulses longer than 2-3 µs, excess energy is spent in gas heating up to 7000 K. Few µs (both ON and OFF times) have the best efficiency and gas temperatures of about 3000 K are measured at the beginning of the pulse. Power modulation and appropriate gas flow residence times allow dissociating CO_2 also in the power-OFF phase and therefore to optimize the efficiency of the process. 2D cylindrical symmetric simulations of the plasma torch give insight in the gas flow dynamics and estimation for a gas residence time in the plasma volume. The gas in the regimes with OFF times close to or longer than the residence time leads to under-processing of the CO_2 flow. The plasma is destabilized by the gas flow itself depending on pulsed regime. The combination of capacitive coupling for ignition (confirmed by frequency harmonics generation) and inductive power absorption lead to complex plasma dynamics where the gas flow affects the impedance matching between the two modes and therefore the plasma efficiency for CO_2 dissociation.

1 Introduction

Energy efficient conversion of CO_2 molecules into fuels is an attractive option for renewable energy storage as well as for mitigation of greenhouse gases emissions (e.g. closing the carbon cycle). Among the variety of Power-to-X solutions, chemical synthesis of energy carriers using plasmas show high potential for the efficient use of intermittent renewable energy sources. To date, the highest efficiency of the plasma assisted conversion of CO_2 into CO is reported in experiments with microwave-sustained plasmas [1-4]. The compact microwave plasma applicators are well investigated in many experiments. Among them, the systems which are proposed for gas conversion [5], surface treatment [6, 7], film deposition [7, 8], disinfection [9, 10], cell treatment[11, 12]] and miniature plasma thrusters [13]. The compactness of applicator is usually enabled by its configuration: either micro-strip [8] or coaxial [7, 9, 10, 14]. Particular for the gas conversion systems, which are operated not with noble gases but rather with stable molecules, e.g. CO_2 and/or N_2, at atmospheric pressure, the coaxial design is more appropriate for operation at low powers (< 1kW). It is conditioned by the fact,that the reaction products need to be enclosed within a narrow tube where the plasma is ignited and processes the gas flow. Many recent studies have been focused on the investigation of microwave plasma torches for gas conversion and more particularly for CO_2 valorization at moderate pressures up to atmospheric conditions[15-20].

The efficiency of the process can potentially be promoted by pulsed supply of microwave energy into the plasma discharge in short pulses with a modulation time shorter than characteristic vibrational-to-translational energy transfer times. In atmospheric pressure plasmas, the demand on the speed of energy pulsations is much higher than at vacuum conditions because of the higher collisional frequencies [21] .

Recently, we have reported on the beneficial effect of pulsation on CO_2 splitting with atmospheric pressure microwave plasma [19] . We found evidence of the promotion of non-equilibrium plasma states and of quenching of the gas temperature enabled through the control of pulse and inter-pulse times. The time evolution of gas temperature measured with ultra-fast optical emission spectroscopy (OES) correlated well with the conversions expected by thermal equilibrium for a pulse of 2.5 μs. Under those pulse conditions vibrational and rotational dynamics revealed that c.a. 1.6 μs are necessary to reach Vibrational-Translational (VT) equilibrium.

However, what is the effect of other pulse conditions on the efficiency and conversion? If thermal processes seem to rule the CO_2 conversion in MW plasmas, would other pulse conditions favor such reaction?

In order to answer these questions, here we analyze the CO_2 conversion under a systematic scan of pulse conditions (duty cycle and pulse times). The effect of pulsation on efficiency is analyzed in terms of not only chemical conversion, but also in terms of the time resolved coupling efficiency of the power to the plasma. Its impedance variation during the pulse is evidenced by the amount of microwave power absorbed while keeping the same electrical characteristics of the generator (driving frequency and load) and impedance of the matching circuit. Some effects of power pulsation and its interplay with the gas flow are highlighted together with their consequences on the efficiency of the process and stability of the plasma. The VT equilibrium is also analyzed by optical emission spectroscopy. With this work, critical aspects are identified in CO_2 conversion that, when addressed, will allow to improve future torch designs.

2 Experimental Methods

2.1 Experimental set-up

The schematics of the experiment and diagnostics are sketched in Figure 1. The solid-state microwave generator HY-2016 can operate at frequencies between 2.4 and 2.5 GHz with a step of 10 kHz [22]. The maximum output power is of 300 W which can be supplied either as a continuous wave (CW) or in pulses. In the pulsed operation mode, the ratio of peak power (power in the pulse) to the power in between pulses is higher than 99, the power rise and fall time are about 5 ns. The duration of pulse time (t_{on}) and inter-pulse time (t_{off}) can be controlled independently from 50 ns to 200 μs with a minimal step of 10 ns. The duty cycle, $DC=t_{on}/(t_{on}+t_{off})$, can be varied correspondingly between 2.5E-4 and 0.9998. The solid-state microwave generator has a coaxial 50Ω N-type output and is connected to the microwave plasma torch by means of coaxial cable. Between microwave generator and plasma torch a bi-directional coaxial coupler (-30 dB) is installed to branch the input and reflected powers from the supplying line and guide them to the power detectors.

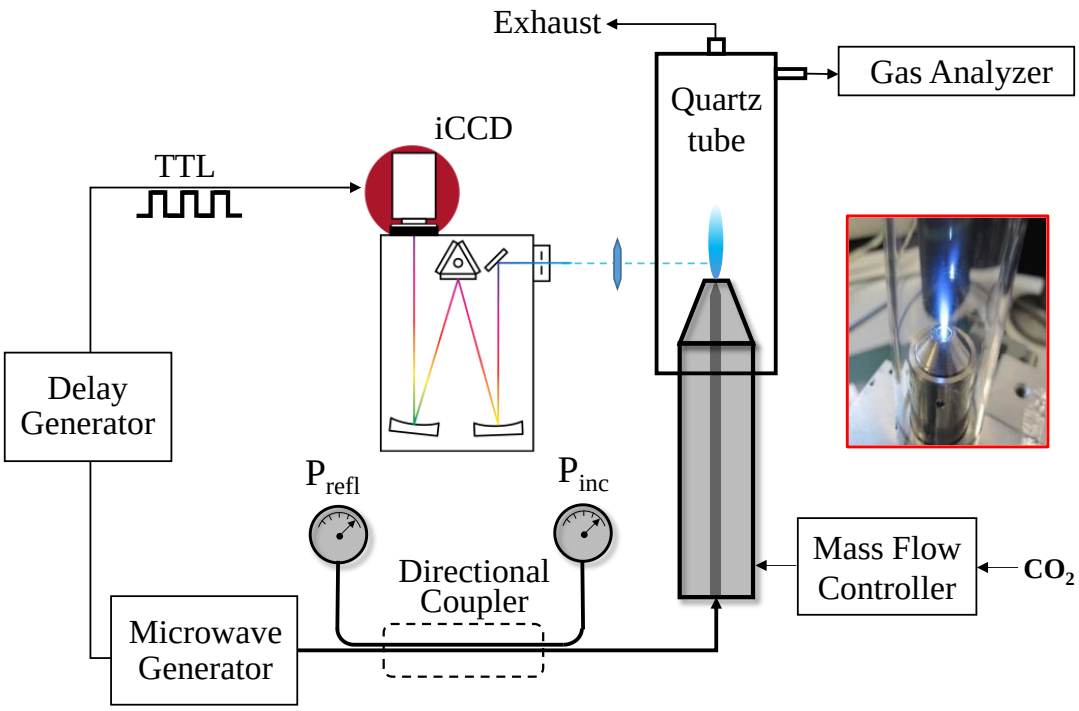

Figure 1. Scheme of the experiment with diagnostics and controls used.

The industrial coaxial atmospheric plasma torch PS-Cle from Heuermann HF-Technik GmbH serves as a plasma reactor in present study (Figure 1) [23]. The working gas flows between inner and outer coaxial conductors in the torch. The outer electrode has a transition from cylindrical to conical shape at its end, which narrows the gas flow channel and forms the nozzle configuration. The inner electrode has also a conical form at its end. The gap between inner and outer electrodes is minimal near the opening of the torch that enables concentration of electromagnetic field and spontaneous ignition at a frequency of 2.49 GHz and at a supplied microwave power of 150 to 180 W. After plasma is ignited, the 2.49 GHz is not anymore optimal from point of view of impedance matching between plasma and supplying line, and the frequency of the generator is set back to 2.45 GHz. The gas supply in the torch is organized through the side input (4mm OD) in the lower part of the torch, which is not symmetrical with respect of coaxial geometry of electrodes. However, the microwave port is aligned with the central electrode. For evaluation of concentration of the reaction products, the torch is surrounded with a quartz tube whose inner diameter of 26 mm is much bigger than the transverse size of plasma plume (1-2 mm in diameter) that means that the plasma flow is not influenced by the quartz tube (see Figure 1).

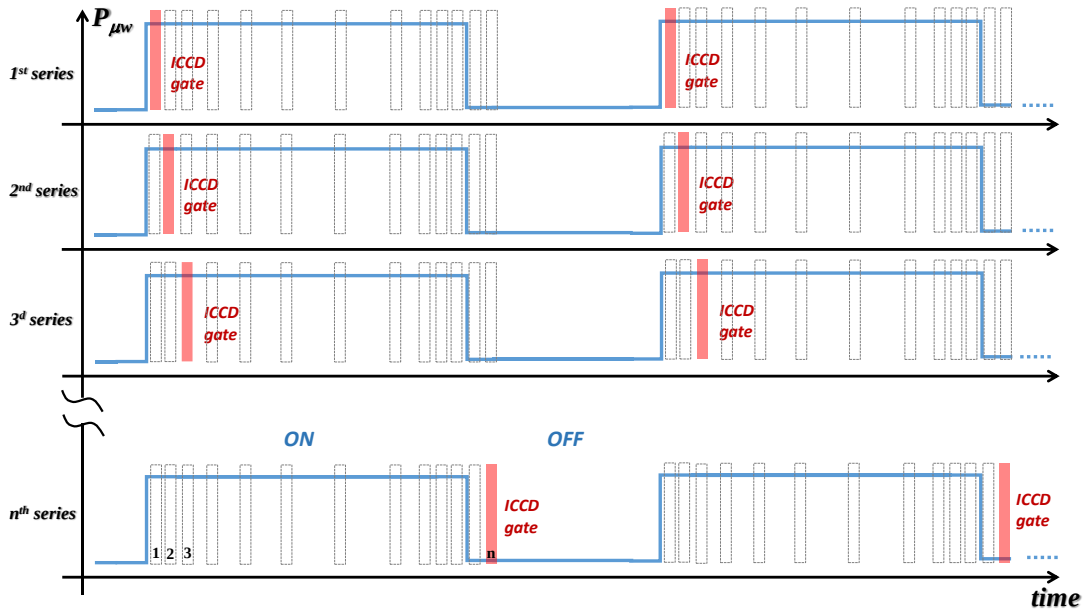

Figure 2. Scheme of acquisition for time resolved OES in plasma sustained with pulsed microwave. The solid, thick rectangular line sketches the microwave power pulse. The red filled rectangles indicate the gate interval of ICCD camera which is shifted with respect to the pulse start in every next series of acquisitions (1, 2, …,n). The dashed grey rectangles indicate the gates in all acquisition series.

2.2 Nanosecond time resolved Optical Emission Spectroscopy (OES).

For estimation of vibrational and rotational temperatures in plasma reactor, the optical emission spectroscopy is utilized. The spectrometer consists of high-resolution spectrograph Acton SP-2756 with 750 mm focal length and intensified (ICCD) CCD camera from Andor, (type A-DH340-18U-03), with a chip size of 512×2048 pixels and a pixel size of 13.5 μm. The spectrometer was calibrated in wavelength as well as in signal intensity together with the ICCD camera, the lens and fiber optic cable. For the wavelength calibration and for relative intensity calibration, the mercury lamp (from Princeton Instruments) and the USB-LSVN VIS-NIR lamp (from Princeton Instruments) were used, respectively. With a small lens (6 mm in aperture), the light emitted from the central part of the plasma discharge is collected and guided by an optical fiber to the entrance of the spectrograph. The grating used in the present work is a holographic type grating with 1800 lines per mm, which provides a spectral resolution of about 25 pm. The ICCD camera features the ultra-fast gating time (>2 ns) that enables the acquisition of emitted light within a single microwave pulse with nanosecond time resolution. To have a statistically significant signal at short gating times, the accumulation modus is always necessary. To sum the collected light in phase with a microwave pulse, the gate of the ICCD camera is synchronized with the microwave pulsation by means of output TTL signal from microwave source and a digital delay generator (SRS DG 645) (see Figure 1). When being triggered by the signal coming from microwave source, the DDG generates a trigger for the ICCD camera with a definite delay. By varying this delay time, the ICCD gate can be precisely (±10 ps) linked to a definite phase of the microwave pulse thus enabling phase resolved acquisition (see Figure 2). In present study, 200 acquisitions with a gate width of 50 ns are used. Such a setup has enabled a unique spectral characterization of a plasma discharge within a single period of microwave power modulation with a time resolution of 50 ns.

2.3 Time Resolved Measurement of Absorbed Microwave Power.

For evaluation of the reaction efficiency, the accurate measurement of the absorbed power in the plasma is necessary. Moreover, given the dynamic nature of delivered power, it is convenient to use a time resolved method to study the microwave absorption efficiency. Thus,

for the evaluation of both incident and reflected power, the real-time power sensors RTP5006 from Boonton Electronics were utilized [24]. These sensors allow to measure the power time profile with any width >10 ns and rise/fall time >3 ns. Since the power pulse-form deviates from an ideal rectangular shape (especially in the reflected power signal) the power signals were recorded and integrated in Matlab to calculate the absorbed power as follows:

$$P_{abs} = \frac{1}{T}\left(\int_0^T P_{inc}(t)dt - \int_0^T P_{ref}(t)dt\right) \qquad (1)$$

Here, P_{abs}, P_{inc}, P_{ref} and T are the absorbed power, incident power, reflected power and the period of power modulation $T=(t_{on} + t_{off})$, respectively. The P_{abs} obtained using eq. 1 was used for the determination of the process efficiency values presented in chapter 3.1. The time resolved reflected power signals $P_{ref}(t)$ serve for the estimation of degree of impedance mismatch at different pulsation parameters presented in chapter 3.2.

Note, the leakage of microwave power from the reactor measured with a microwave leakage detector is below 1 mW/cm^2 at a distance of about 5 cm away from the torch end. Therefore, it is taken as negligible for estimation of absorbed power in plasma.

3 Experimental results and modelling

3.1 Finding optimal operation windows in parametric space

To optimize the CO_2 dissociation reaction for the given coaxial plasma torch in atmospheric pressure, we have performed a systematic variation of pulse parameters of supplied microwave power. The aim is to find the optimal operation window, where conversion and efficiency are maximal. Throughout all measurements, we kept a CO_2 gas inflow as high as 12 slm. Note, that in the present experiments, the peak power (P_{peak}) deviates by ± 13% around 265 W mostly depending on duty cycle (0.10<DC<0.67) because of a not fully compensated temperature drift in the amplifier of the solid-state source.

To enable a comparable analysis of the data, for every chosen parameter set, the specific energy input (SEI) based on the absorbed power in plasma torch (P_{abs}) is calculated. Therefore, SEI reads as follows:

$$SEI = \frac{P_{abs} \cdot V_m}{\nu_{inp} \cdot N_A}, \qquad (2)$$

where ν_{inp}, V_m, and N_A are the CO_2 gas inflow, molar gas volume (24.47 L/mol) and Avogadro constant, respectively. The power absorbed in plasma, P_{abs}, is calculated on the base of time resolved measurements of the reflected and incident powers and equation (1).

For a pulsation regime, a 14×14 (t_{on}; SEI) parameter matrix was defined. The pulse time is varied from 0.050 µs to 30.00 µs. Moreover, t_{off} time is varied in such a way that to have a DC varied approximately between 0.1 and 0.7 for every single t_{on}. Thus, the specific energy input resulted from variation of t_{off} time varies from 0.02 to 0.15 eV/molecule. Each point in the parameter matrix was measured randomly, three times, in order to estimate statistical deviations in the measured parameters. Moreover, measurements in CW mode at different input microwave powers were also performed. This has enabled the comparison of pulsation mode against CW mode for the same SEI values.

The molar degree of CO_2 conversion into CO, χ, as well as the process efficiency, η, are plotted both for pulsed and for CW regimes along corresponding SEI values in Figure 3. Here, the efficiency reads as follows:

$$\eta = \frac{\chi \cdot \Delta H_R^0}{SEI}, \quad (3)$$

where ΔH_R^0 is the reaction enthalpy, which is 2.93 eV/molecule.

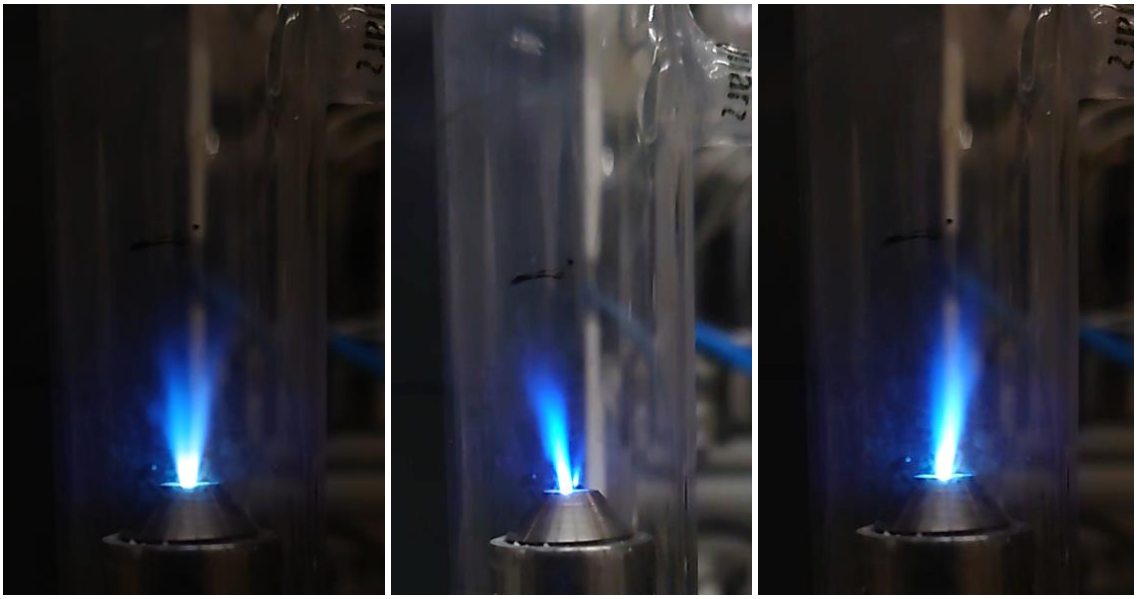

Figure 4. Evidence of plasma instability and plume shape variation with the pulse regime. a) t_{on}=1.0 μs, t_{off}=2.61 μs (V-shape); b) t_{on}=2.0 μs, t_{off}=6.67 μs (bent); c) t_{on}=2.0 μs, t_{off}= 2.44 μs (shake).

It is observed that in each case the pulsation improves both conversion and efficiency as compared with continuous (CW) energy supply. This verifies the previously identified improvement of conversion of CO_2 in microwave plasmas with ultrafast pulsation [19]. The CO yield remains approximately in the range of 1% because of the low SEI corresponding to a large gas flow, required to operate the plasma without overheating the components of this kind of torch and the small volume of the plasma as compared to the cross section of the outlet of the torch. The reactor gas outlet is 4 mm in diameter, though the plasma itself is about 2.0 to 2.5 mm in diameter and about 10 mm in height.

There is a clear trend of increase in statistical deviation for the conversion values for which the efficiency is bigger (Fig 3 a). Two fully independent campaigns of measurements were performed to check the increase of statistical spread around the mean values. Both the mean values and larger distribution of conversion values were confirmed. And the results are similar to the ones published in a previous work with a replica torch [19].

One of the possible explanations for a bigger statistical deviation in the most advanced pulsed regimes is the plasma flow instability arising from the turbulent nature of plasma flow driven by the nozzle geometry and the sustaining power pulsation. Even visually (see Figure 4 and Supplementary video) it can be observed that in some regimes the plasma shape is not along the symmetry axis and/or shudders laterally. This observation can be connected to plasma instabilities reported for other atmospheric microwave plasmas [25, 26]. The reported sources of such instabilities include the electric field, flow effects or the filamentary nature of atmospheric plasmas [25]. It should be noted, that the plasma plume shapes shown in Figure 4 are reproducible for given pulse parameters.

In addition, the energy pulsation can also destabilize the plasma if the characteristic pulsation times are comparable with the gas residence time in the reactor zone. Under energy pulsation regime, the interchange of heating and quenching (because of mixing with surrounding atmosphere) may result in space gradients of temperature and of charged particle concentrations in plasma flow, which may drive its instability. Additionally, the degree of CO_2

conversion governs the concentration of negative ions which in its turn influences the electric field that maintains the plasma and also can be a driving force for instabilities.

Another consequence of the interruption of supplied energy takes place when the t_{off} is longer than the residence time. In that case some amount of gas “does not see” any microwave plasma. Yet in that case, the gas is somewhat activated by the plasma afterglow which is much less effective than the plasma itself. Thus the critical condition is when the number of microwave pulses during the residence time is around one.

To estimate the gas residence time and to gain a better understanding on gas flow dynamics in the studied coaxial torch, we have utilized the Computational Fluid Dynamics (CFD) solver available in COMSOL. We have considered atmospheric pressure, 12 slm of CO_2 inflow and net heat power of 200 W as input parameters. The heat source profile is approximated with a Gaussian function with the maximum 1 mm above the torch end (Fig. 5 a), which corresponds to the maximum of emitted light intensity in experiment. In Figure 5 b-d the resulted gas velocity magnitude, the radial component of flow velocity and temperature are presented. It is found, that approaching the nozzle the axial gas velocity increases rapidly from 4 m/s to 22 m/s. At the same time, just above the torch end, where the energy coupling is assumed, the gas velocity is about 20 m/s. Note, that near the nozzle coordinates, the radial component of gas velocity is comparable with the axial component (-10 m/s) and directed to the axis of torch which is a common velocity feature for nozzles (Fig. 5 c). It should be noted that at T>2500 K the dissociation of CO_2 takes place and heat capacity as well heat conductivity and viscosity of resulted gas mixture can differ from the predefined ones for CO_2 in the present model.

From the above simulated gas velocity of about 20 m/s and an estimated length of the reactive region between 1 mm and 5 mm, we evaluate a residence time as high as 50 to 250 µs. As it was abovementioned, the regimes with the inter-pulse times of the order of or longer than 50 µs (for present set of parameters are the regimes with t_{on} > 10 µs) can be additionally unstable.

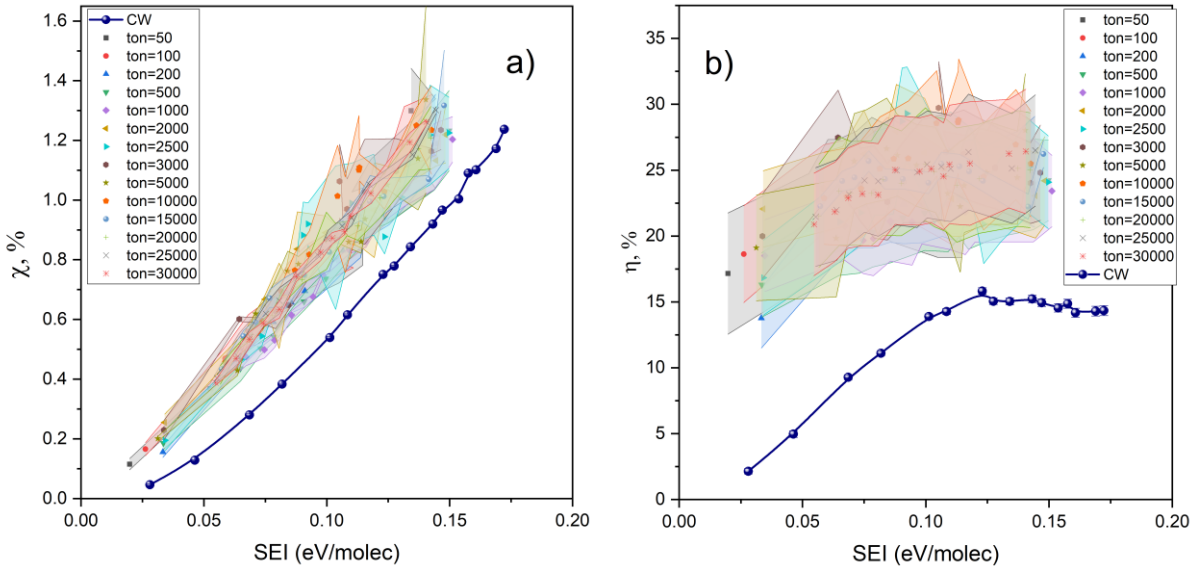

Figure 3. Conversion (a) and efficiency (b) for different pulse times (t_{on}) and duty cycles. The data measured in continuous wave (CW) regime and at different input powers are shown as reference. Discharge parameters: CO_2 flow is of 12 slm, P_{peak}=265±35 W, p=1 atm, 0.10<DC<0.67.

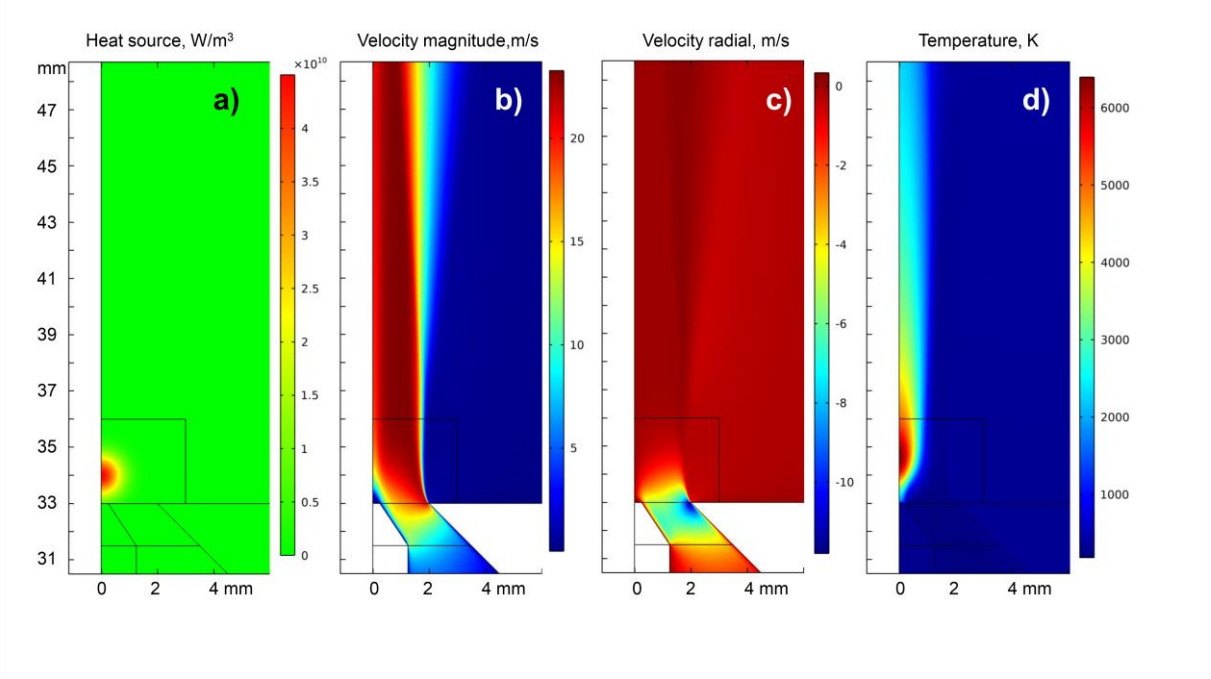

Figure 5. Computational Fluid Dynamics (CFD) model for 12 slm CO_2 gas inflow and net heat power of about 200 W at p=1 atm. a) Heat source: Gaussian profile with maximum of 4.5E10 W/m^3 , b) flow velocity magnitude, c) radial component of flow velocity, d) temperature.

Given the above-mentioned fluctuations, some pulsation regimes from the parameter scan would not be reproducible enough to provide an analysis leading to predictable behavior of the plasmas. Thus, to identify the most efficient parametric space for a chosen operation condition and at the same time, perform the analysis on the stable regions, the conversion and efficiency is plotted in (SEI-t_{on}) coordinates in semi logarithmic scale in Figure 6. The measured conversion and efficiency are shown as solid circles whose color is ranged along the conversion or efficiency scale accordingly. Additionally, the regimes where plasma was unstable are marked with the open black squares. Dashed lines sketch the regions with maximal conversion (Figure 6 a) or efficiency (Figure 6 b). Note that the efficiency is calculated on the base of absorbed microwave power in the plasma torch and has to be understood as a chemical efficiency, which is higher than the reactor efficiency (see section 3.2).

The conversion shows an increasing trend with SEI, thus, within a chosen parameter space the conversion is generally promoted by the average power supplied to the plasma. Nearly no dependency of conversion on the t_{on} is recognized for any given fixed SEI. For the calculated efficiency (Figure 6 b), it is observed the same trend with the SEI as for conversion excepted for an apparent increase in scattering of the data due to normalization to absorbed power. The region with SEI>0.09 eV/molecule which is optimal for the conversion is highlighted with dashed line in Fig. 6 a. The optimum region for efficient CO_2 conversion is found and sketched roughly with a dashed line in Fig. 6 b: 2 µs<t_{on}<5 µs, 0.07<SEI<0.11 eV/molecule which is similar to one already published in [19].

As to the stability of plasma plume, we see the following trend: in the regimes with high efficiency, plasma is often unstable. It is difficult to judge whether the instability promotes higher conversion or, vice versa, the higher conversion attained at the optimum pulse parameters promotes the instabilities of plasma. This will be studied in next works, and we do not go further in depth in that topic in the present account.

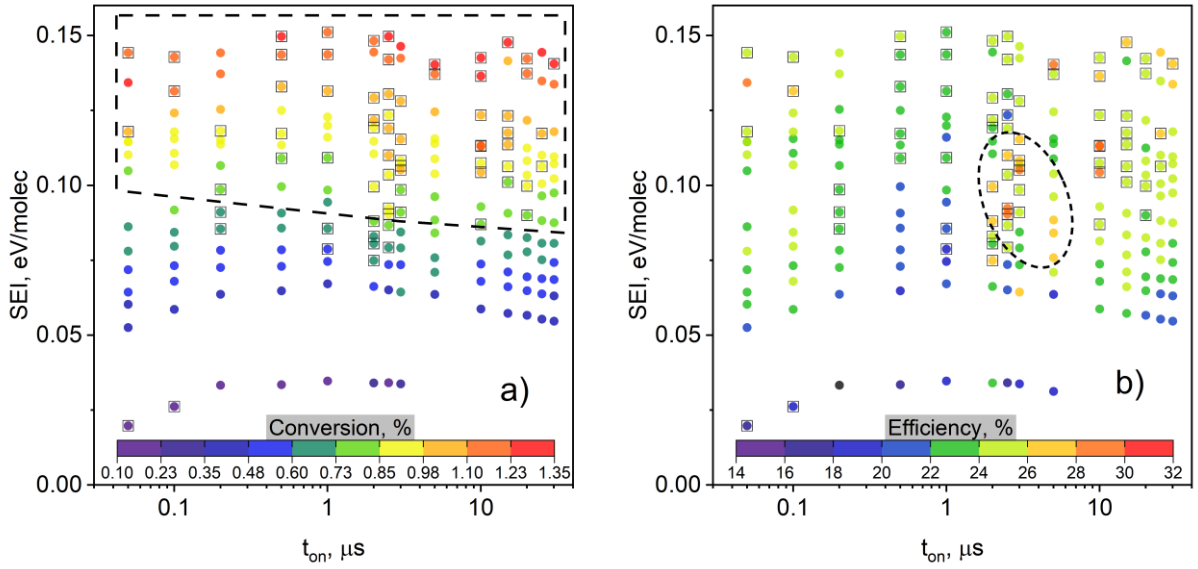

Figure 6. Conversion (a) and efficiency (b) for varied SEI and pulse time (t_{on}). The measured magnitudes are color-coded. The unstable regimes are indicated additionally with open squared symbols. Dashed lines sketch the maximal conversion and efficiency regions. Discharge parameters: CO_2 flow is of 12 slm, P_{peak}=265±35 W, p=1 atm, 0.10<DC<0.67.

3.2 Power absorption in plasma

The coaxial torch may be considered as a coaxial line and plasma serves in that case like an electrical load. Depending on plasma conductivity, it can absorb a given amount of supplied microwave energy, and the excess will be reflected back. Since the electron density in the afterglow reduces exponentially with time after the pulse end, the plasma re-ignition with next microwave pulse may also take place at a different time because of the required time to restore the steady state electron density value. As the impedance of the generator and coaxial line were kept constant throughout all investigated regimes, the time traces of reflected power can therefore serve as an indicator for the electron density development in the discharge.

We have investigated both the incident and reflected power in the system with real-time power sensors connected to the ports of an installed bidirectional coupler. The reflected power (P_{refl}) traces are shown in Figure 7 where we compare three regimes with DC=0.20, DC=0.33 and DC=0.67. The initial dynamic in all regimes is similar: P_{refl} increases during the first 5 to 20 ns because of lack of charge carriers in the plasma afterglow. Since the front of the incident pulse is about 10 ns, the input power grows at approximately 25 W/ns, whereas the absorbed power is assumed to be also increasing due to growing electron density. After the input power pulse reaches a plateau, the dynamic of P_{refl} is either falling (see all traces in DC=0.20 and DC=0.33 in Fig. 7 a and b) or constant (see regimes with t_{on}=0.1 and 0.5 μs in Fig. 7 c). The first one reflects further re-establishing of electron density in plasma, and the second dynamic evidences that the formation of electron density is already completed, and in that state, plasma impedance results in P_{ref}≈60 W. Interestingly, this level of 60 W is universally attained in later times of pulse in all regimes where t_{on} is long enough.

Remarkably, in many regimes the P_{refl} between the start of its falling, in the beginning of pulse, and attaining the ≈ 60 W level, in the end of pulse, has a minimum ranging between 20 and 25 W. It means that in those periods P_{abs} is maximal. The time coordinate of that minimum in series with DC=0.20 and partly DC=0.33 (for t_{on}>10 μs) is close to 2 μs. This time agrees well with the time found for equilibration of gas temperature, T_{gas}, with vibrational temperature, T_{vib} in regime with DC=0.25 [19]. Note that in the regime with DC=0.67, this minimum is attained

earlier, between 0.03 and 0.07 μs (Figure 7 c), that might result from an earlier T_{gas}-T_{vib} equilibration caused by the shorter t_{off} times. This effect can be related to temperature development during the pulse, but more a dedicated study is needed to explore it in details.

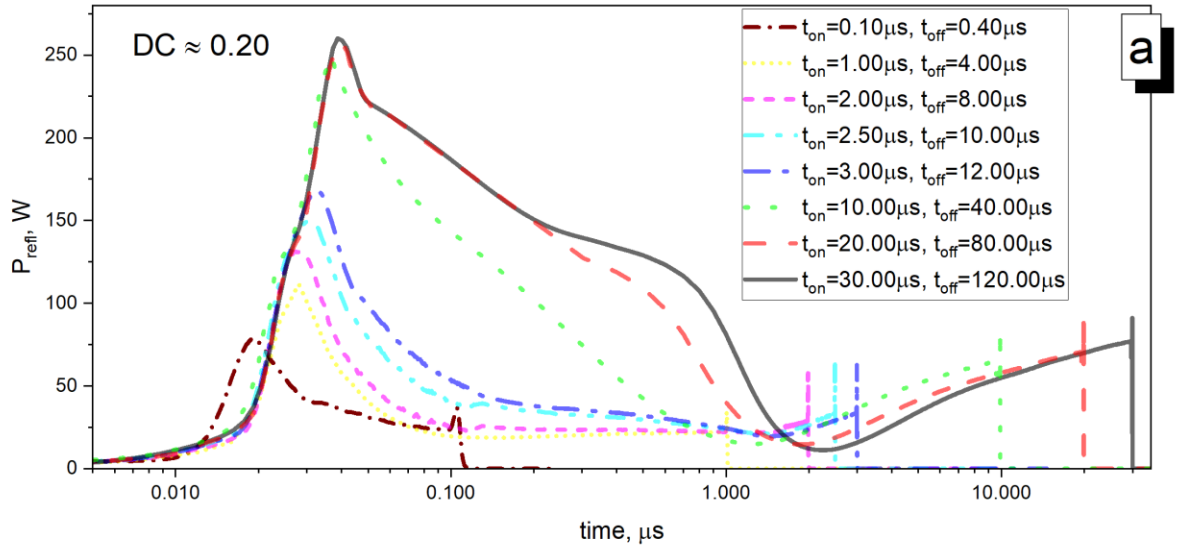

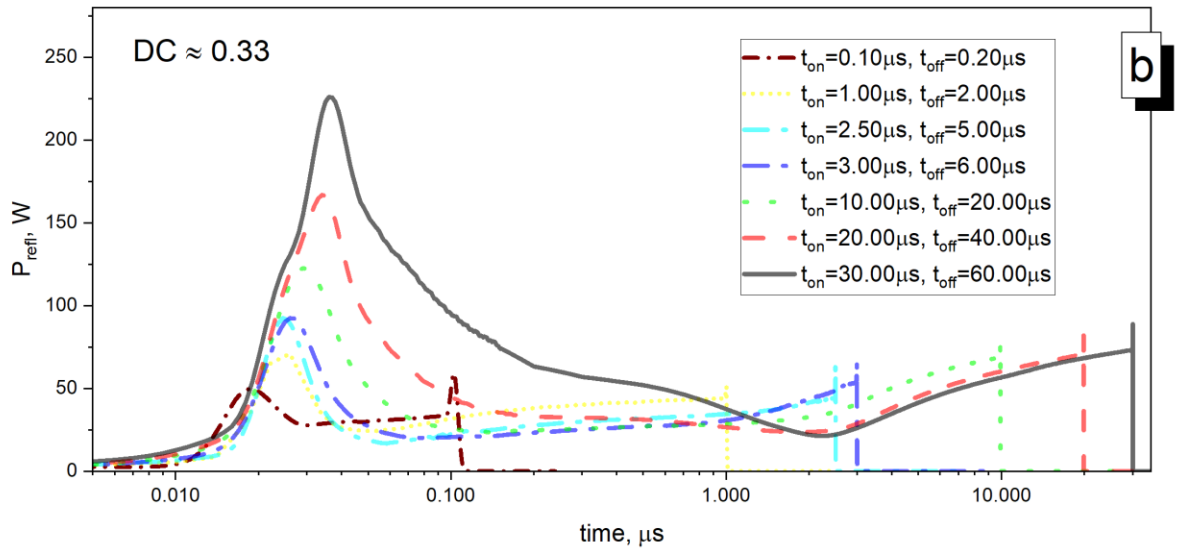

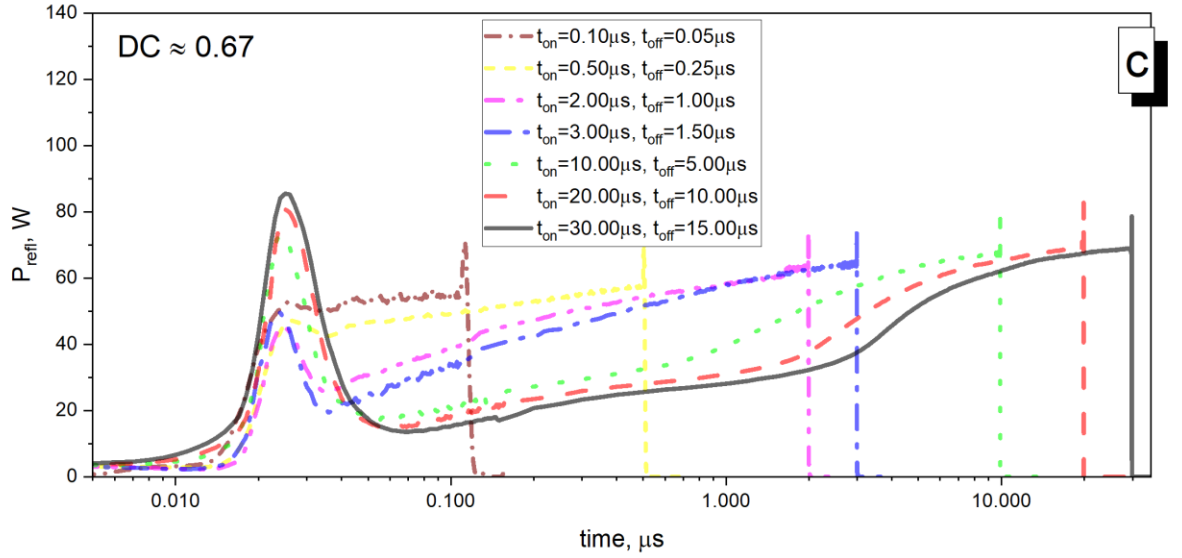

Figure 7. Reflected microwave power in regimes with a) DC=0.20, b) DC=0.33 and c) DC=0.67. CO_2 inflow is of 12 slm, P_{peak}=265±35 W.

It is worthwhile to note that the amplitude of the first peak in P_{refl} traces in Figure 7 correlates clearly with the t_{off} times: the longer t_{off} the more power reflected back in the beginning of pulse and vice versa. It supports the idea that the initial dynamic of P_{refl} is defined by the leftover electron density, which is dependent on the length of the OFF phase.

3.3 Rotational and vibrational temperatures

As mentioned earlier, a complete picture of the plasma behaviour require not only of an observation on the electric field but also on the plasma temperature. Moreover, the observation of the VT equilibrium in a wider set of pulse conditions will help us feed the set of conditions for an optimal reactor design.

To characterize the state of VT non-equilibrium, the acquired emission spectra are used to obtain the vibrational (T_{vib}) and rotational (T_{rot}) temperatures by fitting of the molecular bands of CO and C_2 species with synthetic spectra using MassiveOES [27]. We assume also in the following analysis, that rotational and gas temperatures are equivalent ($T_{rot} \approx T_g$) due to sub-nanosecond rotational−translational relaxation at atmospheric pressure [28].

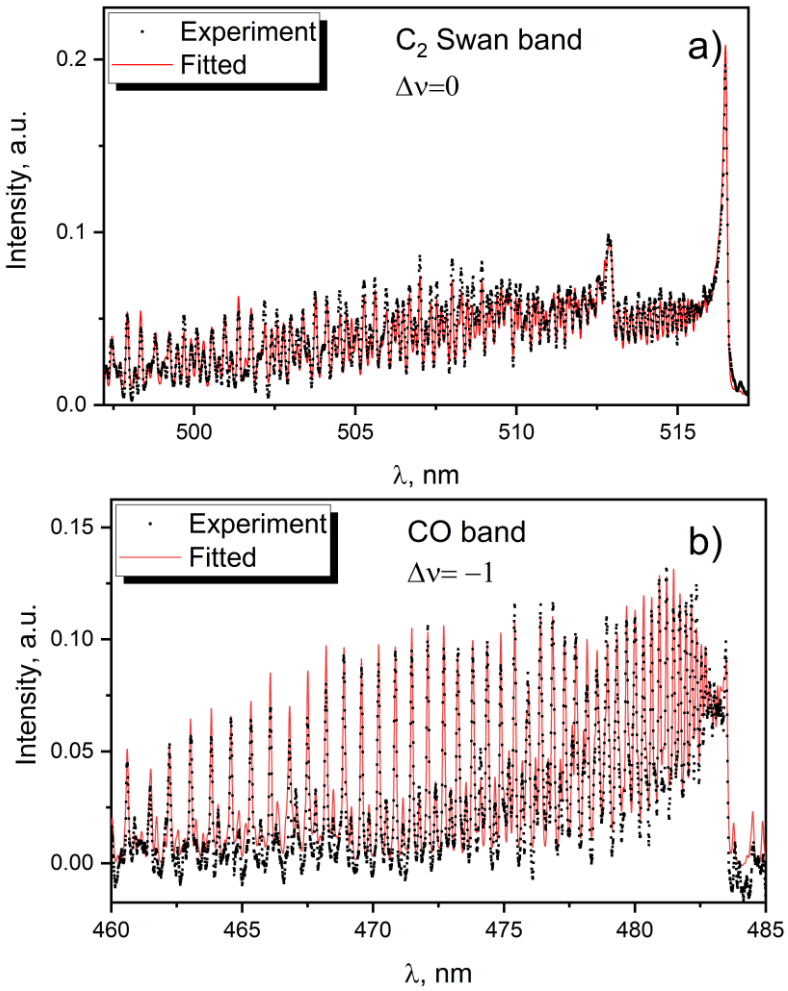

Figure 8. Two examples for fitting of experimental plasma emission spectrum with one synthesized in MassiveOES program: a) C2 Swan Δν=0 band, b) CO Angström Δν=-1 band.

The vibrational and rotational temperatures of heavy plasma species are defined with MassiveOES [27, 29] software, which fits the experimental molecular bands with the synthetic spectra. For the fitting, the database for the C_2 ($d^3\Pi_g - a^3\Pi_u$) Swan bands system by Brooke

et al with recent compilation and calculations [30] included into MassiveOES is used [31]. In the beginning of the pulse, the CO Angström bands usually dominate the spectrum and for them, the line-resolved emission probability is calculated employing programs LEVEL [32] and PGOPHER [33] and utilizing the molecular constants from [34-37]. It is also assumed that for the present conditions, a Boltzmann distribution is valid [31]. A typical result of fitting for experimental C_2 Swan and CO Angström bands are presented in Figure 8. The systematic errors (baseline and baseline slope) give the largest contribution in the uncertainties for T_{vib} and for present data are estimated as ±1000 K. Due to fact that the simulated spectra are sensitive to T_{rot} in a much broader wavelength range, the uncertainties for the T_{rot} are smaller at least by factor of 2.

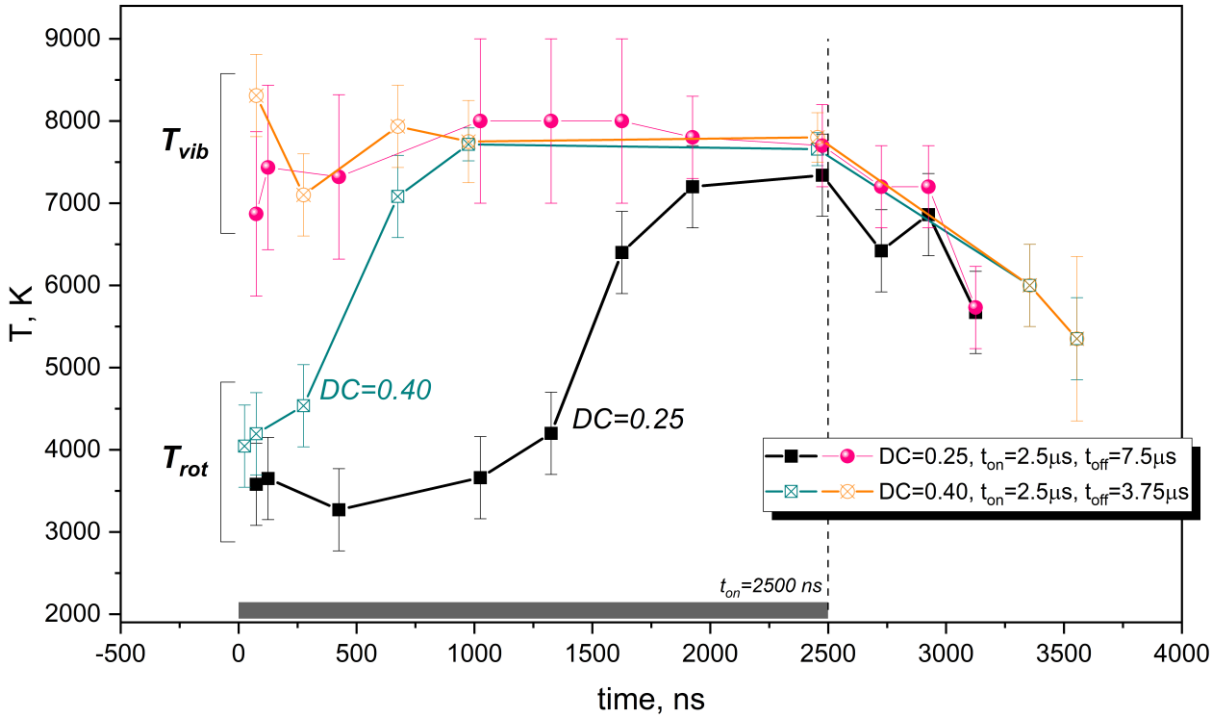

Figure 9. Comparison of dynamics of rotational (T_{rot}) and vibrational (T_{vib}) temperatures in pulsed regime with t_{on}=2.50 µs, t_{off}=7.50 µs (DC=0.25) against t_{on}=2.50 µs, t_{off}=3.75 µs (DC=0.4). Parameters: CO_2 inflow is 12 slm, P_{in}=220 W.

Figure 9 shows the evolution of T_{vib} and T_{rot} along the 2.50 µs pulse in two experiments with different t_{off} times: 7.50 µs (corresponds to DC=0.25) and 3.75 µs (corresponds to DC=0.40). As we have reported before [19], two distinct regimes exist along the energy pulses: a non-equilibrium regime at the beginning of the pulse (T_{vib}>T_{rot}) and a thermal equilibrium regime when T_{rot} approaches T_{vib}. For t_{off}=7.50 µs, equilibration time is approximately 1.6 µs, though for t_{off}=3.75 µs, the equilibration happens earlier – at about 1.0 µs. This is related to the longer time required for coupling all the power to the plasma due to the decrease of electron density in the afterglow as highlighted by the higher reflected power values at the beginning of the pulse in Figure 7. Moreover, the T_{rot} in the beginning of the pulse for DC=0.40 is about 500 K larger as compared with T_{rot} for DC=0.25. This can be explained by the shorter cooling time between the two power pulses in case of DC=0.40 as compared to DC=0.25. Or in other words, with higher DC values, the mean absorbed power is also higher and this leads to higher mean gas temperatures.

At the very beginning of pulse, the vibrational temperature determined from vibrational states ($B^1\Sigma^+$) of the CO molecules is already quite developed: 6900 K and 8300 K for DC of 0.25 and 0.40 respectively. Such a prompt vibrational activation can be understood from an efficient vibrational excitation of CO and/or CO_2 or by electron collisions [38]. During the pulse, T_{vib} in

both experiments shows a constant behaviour (7000 K < Tvib < 8000 K). After end of pulse, T_{rot} and T_{vib} stay coupled and are reducing with rates of about 2×10^{9} K/s, which are convenient rates to preserve the CO produced and avoid recombination reactions back into CO_2 [39].

The difference in the duration of non-equilibrium state in two regimes with the same t_{on} and different t_{off} can be explained by different electron concentration, n_e, before the pulse start. In pulse regime, the concentration of electrons during the OFF stage relaxes exponentially [40], therefore, the longer t_{off}, the lower concentration of electrons and vice versa. Considering the chain of energy transfers as $E_{microwave}\rightarrow T_e\rightarrow T_{vib}\rightarrow T_{rot}$, the higher n_e results in a lower mean electron temperature that may become more optimal for vibrational excitation of molecules, whose energy, in its turn, is transferred to T_{rot}. In other words, energy transfer improves electron density [41].

The registration of emitted light after the end of pulse was only possible within 625 ns and 1055 ns pulse lengths for DC=0.25 and DC=0.40, respectively. After those times, signal drops below noise level evidencing that all exited states fade away.

Given that the vibrational temperatures demonstrate universal behaviour along the pulse length, we have investigated the dynamic of T_{rot} for different DC and t_{on} times in more details. In Figure 10, the evolution of T_{rot} along the microwave pulse is presented for four regimes:

1) t_{on} / t_{off}=0.50 / 1.50 μs, T=2.0 μs, DC=0.25,
2) t_{on} / t_{off}=1.50 / 4.50 μs, T=6.0 μs, DC=0.25,
3) t_{on} / t_{off}=2.50 / 7.50 μs, T=10.0 μs, DC=0.25,
4) t_{on} / t_{off}=2.50 / 3.75 μs, T=6.25 μs, DC=0.40.

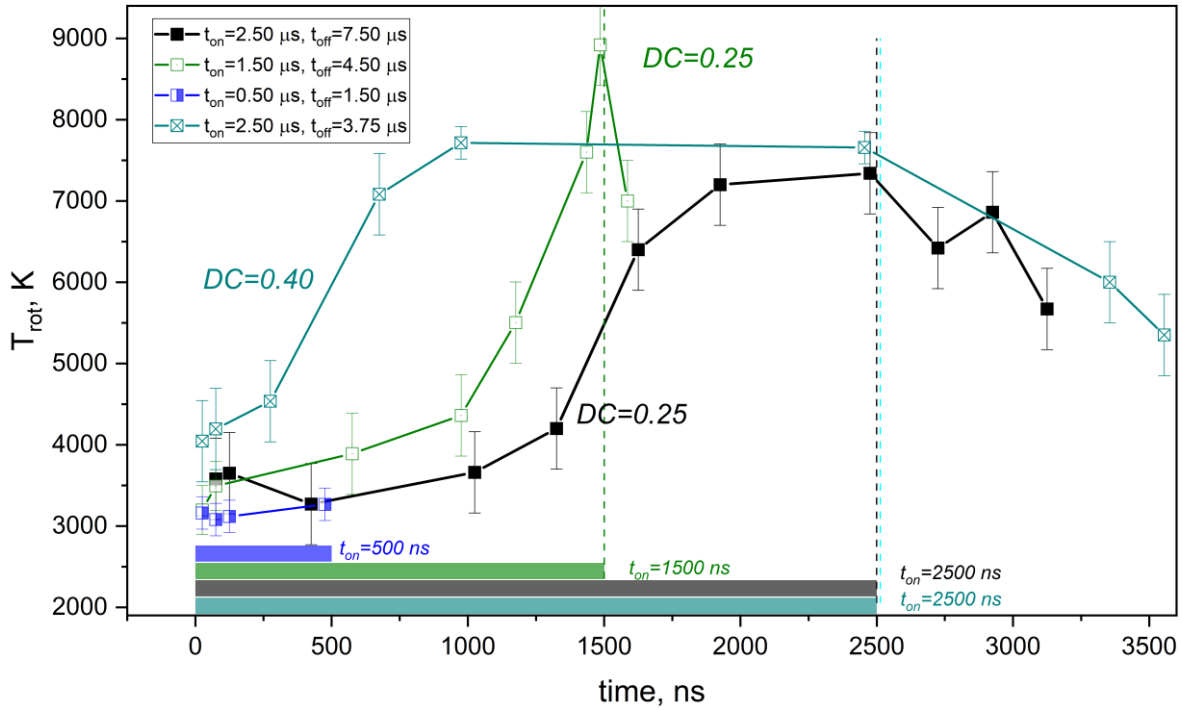

Figure 10. Comparison of dynamics of rotational (T_{rot}) temperature in pulsed regime with DC=0.25 and DC=0.4 at different t_{on}. Parameters: CO_2 inflow is 12 slm, P_{in}=220 W.

The simplest behaviour is observed in the first regime with shortest pulsation times, t_{on}=0.50 μs, t_{off}=1.50 μs, - the gas temperature (half filled squares) linearly grows along the pulse. It is important to mention that in the beginning of the pulse T_{rot} for DC=0.40 exceeds those for all regimes with DC=0.25 by approximately 500 K.

It is interesting to compare the regimes 2 and 3. For the same duty cycle of 0.25, T_{rot} in experiment with shorter OFF phase (t_{off}=4.50 us) shows faster growth as compared with regime 3 with the t_{off} of 7.50 µs. This seems to indicate that higher pulsation frequencies promote higher electron densities and therefore an increase in the heating rate.

3.4 Non-linear interaction of microwave with plasma.

With a plasma, an electromagnetic field can interact via inductive, capacitive or ohmic coupling modes in high pressure discharges. For high electric field conditions, a capacitive coupling of the microwave energy into the plasma is observed via the plasma sheath [42]. In a first approximation, when a plasma reactor is modelled using an equivalent circuit model (i.e. a circuit made of lumped electrical elements), the plasma sheath can be modelled as a capacitor [43]. Indeed, the charge concentration in the thin boundary layer at the plasma edge may be approximated by a capacitor, whose geometry is reactor specific. If the plasma sheaths are not flat and not parallel to each other (as obviously for the present reactor), the energy distribution in such a capacitor will be far from homogeneous. This will lead to the distortion of the temporal form of the field that, in its turn, results in the appearance of higher harmonics in its spectrum.

To explore to what extend the capacitive coupling takes place in coaxial plasma torch, we have measured the electromagnetic spectra near the plasma plume with the aid of a dipole antenna and a signal analyser (Agilent EXA N9010A). In Fig. 11 the spectra with plasma and without plasma (microwave is supplied but plasma is not ignited) are measured at about 1 cm away from the plasma plume. The plasma is sustained in CW mode, with 12 slm of CO_2 inflow, P_{in}=200 W and f=2.45 GHz. As a reference, the signal decoupled from the power line terminated with a matched load is measured at P=200 W and at P=0 and also shown on the same graph. On the right-hand side of Figure 11 the experimental arrangement is shown. Note, in the spectrum of the source, the satellites peaks at +/- 30 MHz and its harmonics are visible at a level of about -60 dBc. Also a weak (-67 dBc) second harmonic exists in the reference spectrum that can be attributed to a very tiny imperfectness in the sinusoidal form of the wave produced by the microwave generator. Interestingly, in the spectrum measured with dipole antenna outside the torch and when no plasma is ignited, the second harmonic of the carrier is absolutely absent, that suggests its full back reflection and absorption in a circulator load in the supplying line.

For the spectrum with plasma, the second harmonic at a frequency of 4.92 GHz is very pronounced (-35 dBc) and prove the existence of the nonlinear interaction. In pulsed operation mode and especially for low DC, the plasma size is smaller than one in CW mode, and correspondingly nonlinear interaction is also smaller as it is seen in Fig. 12. Here, plasma is sustained in pulsed mode with t_{on}=2.5 µs and t_{off}=7.5 µs, at 12 slm of CO_2 inflow, P_{in}=200 W and f=2.45 GHz. It is worth to note, that in this regime, the radiation spectrum of the carrier frequency is not much influenced by the plasma – the spectra are almost overlapped, but the second harmonic at 4.92 GHz is clearly generated when the plasma is ignited.

In Fig.13 the amplitude of second harmonic of the incident wave is plotted for different pulsation parameters and also for CW. The amplitude of second harmonic is approximately proportional to the duty cycle (DC) or mean energy supplied in plasma (see Fig. 13). Measurements for different t_{on} and t_{off} times but similar DCs show similar relative amplitude of the second harmonic of a carrier frequency. The above observations give a strong argument for a capacitive coupling of microwave energy into the sheath which is typical for microwave discharges with strong E-fields [42]. The present measurements do not allow to assess the relative contribution of capacitive coupling as compared to the inductive and ohmic coupling, but shine new insights into the electromagnetic properties of such plasma jets.

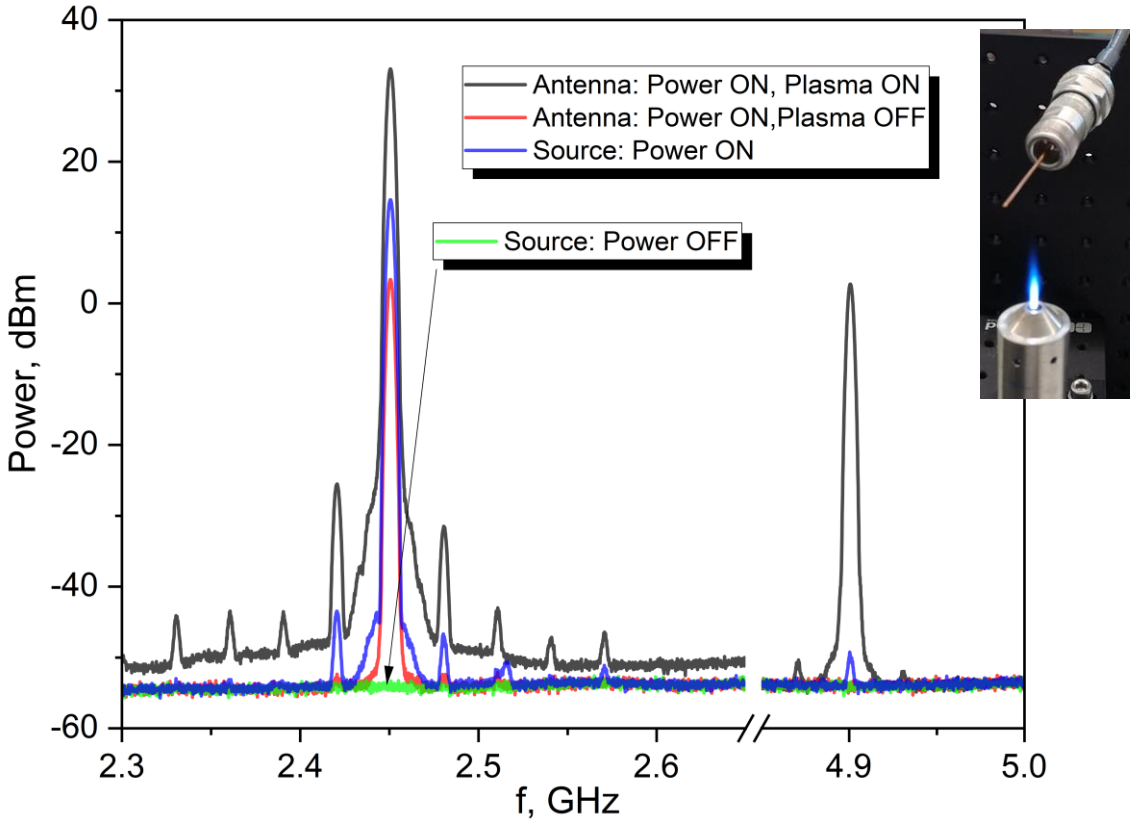

Figure 11. Spectrum of electromagnetic radiation outside the plasma torch (red and black curves) and in the feeding line (blue and green) operated at input CW power of 200 W, and CO_2 inflow of 12 slm. At right hand side: the position of receiving antenna near the plasma torch.

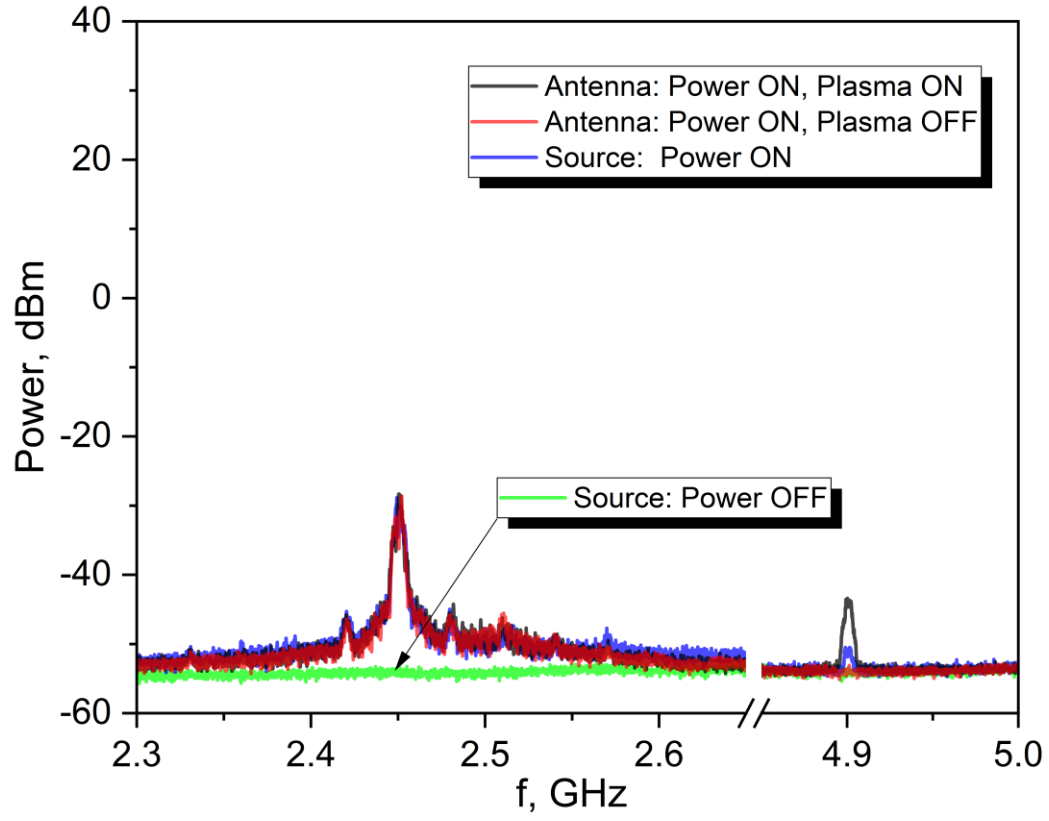

Figure 12. Spectrum of electromagnetic radiation outside the plasma torch (red and black curves) and in the feeding line (blue and green) operated at input peak power of 200 W, t_{on}=2500 ns and t_{off}=7500 ns and CO_2 inflow of 12 slm.

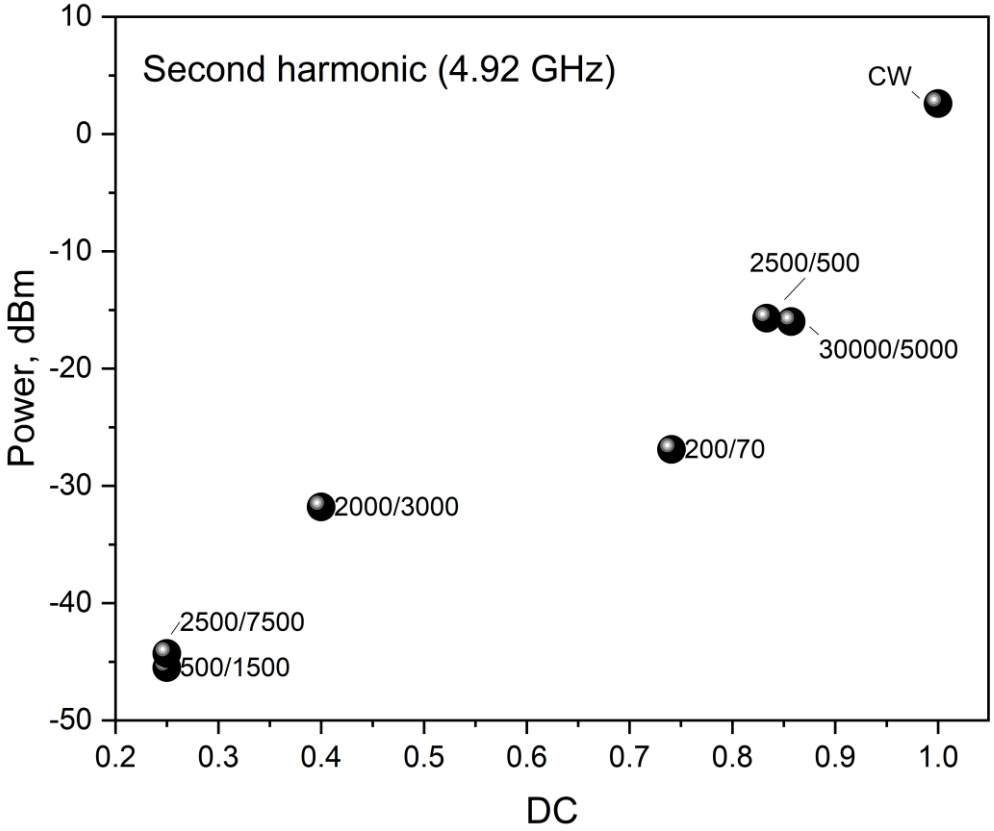

Figure 13. The microwave power at 4.92 GHz (second harmonic of incident wave) acquired with dipole antenna near the plasma torch when the plasma is operated in pulsed and CW regime. The corresponding t_{on}/t_{off} times (ns) are indicated near the data points.

Another phenomenon related to the interaction of strong oscillating electromagnetic fields with a plasma is the so-called parametric instability which is observed via the formation of additional frequency peaks around the frequency of the pumping wave, f_0. Electron volume and surface waves can be excited via coupling to the collective oscillation of ions in the plasmas and are expressed respectively as [42]:

$$f_{pi} = n \cdot f_0 \cdot \sqrt{m_e/M_i} \qquad (4)$$

$$f_{pi} = n \cdot f_0 \cdot \sqrt{2} \cdot \sqrt{m_e/M_i} \qquad (5),$$

where n=1, 2, 3, …, and m_e and M_i are electron and ion mass, respectively. For f_0=2.45 GHz and ^{12}C ions, one has f_{pi} ≈16.5 MHz and 23.3 MHz for volumetric and surface modes, respectively. In the present setup, the side bands are observed with a regular frequency shift of 30 MHz which is approximate agreement with the calculated value. One should note however that the theory assume only the presence of electrons which are very light and that the presence of negative ions would lead to a smaller effective mass ratio between the negative and positive charged species, therefore leading to larger frequency shifts.

4 Discussion and outlook.

Ultrafast pulsations of microwave power sustaining the CO_2 plasmas is a mean to improve the efficiency of the CO_2 conversion into CO and O_2. The detailed scan of the pulsation parameters complemented with plasma diagnostics unravels the underlying mechanisms limiting the CO

yield in the utilized coaxial open-end torch and give way to next-generation torch designs with superior performance.

In general, in the commercial torch used, the active reaction zone is limited to several mm constructively by the geometry of the torch. The minimal flow is 12 slm to avoid any potential damage of the torch due to heating of internal components. Both factors restrict severely the CO yields: for all duty cycles, it is therefore below 1.3% and the study is focused on the efficiency of CO_2 conversion.

At the same time, it is understood that the efficiency of the process depends individually on the t_{on} and t_{off} times. At very short energy pulses, the gas temperature is already high enough (about 3500 K) for thermal dissociation, which is assumed a leading mechanism at atmospheric pressure. However, the plasma volume being very small and the presence of a strong electric field region being unveiled by harmonics generation, electron driven dissociation processes cannot be ruled out.

For longer power pulses, excess energy is spent in gas heating up to 7000 K and dissociation of CO molecules into C and O. The power interruption is useful for temperature quenching but at very long t_{off} times the efficiency is reduced owing to the higher energy cost needed to reignite the plasma. This effect is clearly highlighted by monitoring the reflected microwave power, which cannot be absorbed by the plasma before the sufficient electron density is developed to match the impedance of the generator and plasma torch.

A particularly interesting case is when the pulse duration becomes similar to the gas flow residence time in the plasma volume, which for the present discharge conditions is estimated of 50 µs to 250 µs. 2D cylindrical symmetric calculations, with the plasma modelled as a heat source, give insight in the gas flow dynamics. The calculations indicate that in regimes with t_{off} times comparable or longer than 50 µs, the performance additionally deteriorated because of the gas stream being under-processed.

The most efficient regimes correspond to microwave pulses in the order of a few µs (both ON and OFF times). At these parameters, the pulse length (t_{on}) is long enough to enable both vibrationally (in the beginning of pulse) and thermally (after thermalizing) driven CO_2 dissociation but short enough to avoid overheating; and the inter-pulse length is long enough for quenching and short enough for efficient re-ignition of the plasma. Moreover, some evidence indicating a possible promotion of electron density with pulse frequency has been observed.

In this pulsing range, it is also observed that the plasma is destabilized by the gas flow itself. This can be associated to the formation of temperature and particle concentration gradients during the gas heating and mixing/cooling phases with characteristic times similar but not equal to the pulsing time of the power supply, thus leading to instabilities. The experimental results indicate that the lateral fluctuation of the plasma may actually promote the CO_2 conversion assuming that in average a bigger reaction zone is effectively developed. The increase of statistical errors in the measurements however also stress that characterizing the plasma in such conditions is difficult. The combination of capacitive coupling for ignition (confirmed by frequency harmonics generation) and inductive power absorption lead to complex plasma dynamics and indicate the existence of a high-intensity E field region in the plasma. It remains to be seen if the gas flow affects the impedance matching between the two modes as well and therefore the plasma efficiency for CO_2 dissociation. These effects and theoretical considerations demonstrate that the plasma dynamics in fast pulsed regime present complex spatio-temporal dynamics and are an interesting field for further fundamental investigations in the future.

5 Acknowledgements.

Emile Carbone: acknowledge the support of the Natural Sciences and Engineering Research Council of Canada (NSERC), RGPIN-2021-04363.

6 References.

1. Legasov, V.A., et al., *A nonequilibrium plasma-chemical process of CO₂ dissociation in high-frequency and ultrahigh-frequency discharges.* Soviet Physics Doklady, 1978. **23**: p. 44.
2. Rusanov, V.D., A.A. Fridman, and G.V. Sholin, *CO2 dissociation in a nonequilibrium plasma.* Soviet Physics Technical Physics, 1979. **24**: p. 1195-1198.
3. Asisov, R., et al. *Carbon Dioxide Dissociation in Non-Equilibrium Plasma*. in *Proc. 5th Intern. Symp. Plasma Chemistry*. 1981.
4. Butylkin, Y.P.Z., V.K.; Krasheninnikov, E.G.; Krotov, M.F.; Rusanov, V.D.; Tarasov, Y.V.; Fridman, A.A., *Dissociation of CO2 by a plasma-chemical process in a nonequilibrium microwave discharge.* Soviet Physics - Technical Physics, 1981. **26**(5).
5. Mizeraczyk, J., et al., *Microwave Plasma Sources for Gas Processing.* AIP Conference Proceedings, 2008. **993**(1): p. 287-294.
6. Gregorio, J., et al., *Design of a Microwave Microplasma Source at Atmospheric Pressure.* IEEE Transactions on Plasma Science, 2009. **37**(6): p. 797-808.
7. Yanguas-Gil, A., et al., *Optical and electrical characterization of an atmospheric pressure microplasma jet for Ar/CH4 and Ar/C2H2 mixtures.* Journal of Applied Physics, 2007. **101**(10): p. 103307.
8. Hopwood, J., A.R. Hoskinson, and J. Gregório, *Microplasmas ignited and sustained by microwaves.* Plasma Sources Science and Technology, 2014. **23**(6): p. 064002.
9. Mizeraczyk, J., et al., *Atmospheric pressure low-power microwave microplasma source for deactivation of microorganisms.* The European Physical Journal Applied Physics, 2013. **61**(2): p. 24309.
10. Czylkowski, D., et al., *Atmospheric pressure microwave microplasma microorganism deactivation.* Surface and Coatings Technology, 2013. **234**: p. 114-119.
11. Kang, S.K., et al., *Portable microwave air plasma device for wound healing.* Plasma Sources Science and Technology, 2015. **24**(3): p. 035020.
12. Bogdanov, T., I. Tsonev, and L. Traikov, *Microwave plasma torch for wound treatment.* Journal of Physics: Conference Series, 2020. **1598**(1): p. 012001.
13. Takao, Y., et al., *Plasma Diagnostics and Thrust Performance Analysis of a Microwave-Excited Microplasma Thruster.* Japanese Journal of Applied Physics, 2006. **45**(10B): p. 8235-8240.
14. Choi, J., et al., *Microwave-excited atmospheric-pressure microplasmas based on a coaxial transmission line resonator.* Plasma Sources Science and Technology, 2009. **18**(2): p. 025029.
15. Belov, I., et al., *Carbon dioxide dissociation in a microwave plasma reactor operating in a wide pressure range and different gas inlet configurations.* Journal of CO2 Utilization, 2018. **24**: p. 386-397.
16. Kim, H., et al., *Carbon dioxide conversion in an atmospheric pressure microwave plasma reactor: Improving efficiencies by enhancing afterglow quenching.* Journal of CO2 Utilization, 2020. **37**: p. 240-247.
17. D'Isa, F.A.C., E. A. D.; Hecimovic, A.; Fantz, U. *Performance analysis of a 2.45 GHz microwave plasma torch for CO2 decomposition in gas swirl configuration* arXiv e-prints, 2019.
18. Wolf, A.J., et al., *CO2 Conversion in Nonuniform Discharges: Disentangling Dissociation and Recombination Mechanisms.* The Journal of Physical Chemistry C, 2020. **124**(31): p. 16806-16819.
19. Soldatov, S., et al., *Time-Resolved Optical Emission Spectroscopy Reveals Nonequilibrium Conditions for CO2 Splitting in Atmospheric Plasma Sustained with Ultrafast Microwave Pulsation.* ACS Energy Letters, 2021. **6**(1): p. 124-130.

20. Hecimovic, A., et al., *Enhancement of CO2 conversion in microwave plasmas using a nozzle in the effluent.* Journal of CO2 Utilization, 2022. **57**: p. 101870.
21. Britun, N., et al., *Plasma-assisted CO2conversion: optimizing performance via microwave power modulation.* Journal of Physics D: Applied Physics, 2018. **51**(14): p. 144002.
22. HBH Microwave GmbH. July 2021]; Available from: https://www.hbhmw.de/products/amplifiers.html.
23. Heuermann HF-Technik GmbH. May 2021]; Available from: https://hhft.de/jets-ps-serie.
24. Boonton Electronics Oct 2021]; Available from: https://www.boonton.com/products/rf-power-sensors/rtp5000-real-time-peak-power-sensors.
25. Snirer, M., et al., *Stable filamentary structures in atmospheric pressure microwave plasma torch.* Plasma Sources Science and Technology, 2021. **30**(9): p. 095009.
26. van der Mullen, J.J.A.M., et al., *Single-shot Thomson scattering on argon plasmas created by the Microwave Plasma Torch; evidence for a new plasma class.* Spectrochimica Acta Part B: Atomic Spectroscopy, 2007. **62**(10): p. 1135-1146.
27. Voráč, J., et al., *State-by-state emission spectra fitting for non-equilibrium plasmas: OH spectra of surface barrier discharge at argon/water interface.* Journal of Physics D: Applied Physics, 2017. **50**(29): p. 294002.
28. Carbone, E., et al., *Analysis of the C2 (d3Πg-a3Πu) Swan bands as a thermometric probe in CO2 microwave plasmas.* Plasma Sources Science and Technology, 2020. **29**(5): p. 055003.
29. Voráč, J., et al., *Batch processing of overlapping molecular spectra as a tool for spatio-temporal diagnostics of power modulated microwave plasma jet.* Plasma Sources Science and Technology, 2017. **26**(2): p. 025010.
30. Brooke, J.S.A., et al., *Line strengths and updated molecular constants for the C2 Swan system.* Journal of Quantitative Spectroscopy and Radiative Transfer, 2013. **124**: p. 11-20.
31. Carbone, E., et al., *Analysis of the C_2 ($d^3\Pi_g$-$a^3\Pi_u$) Swan bands as a thermometric probe in CO_2 microwave plasmas* Plasma Sources Science and Technology, 2020. **29**(5): p. 055003.
32. Le Roy, R.J., *LEVEL: A computer program for solving the radial Schrödinger equation for bound and quasibound levels.* Journal of Quantitative Spectroscopy and Radiative Transfer, 2017. **186**: p. 167-178.
33. Western, C.M., *PGOPHER: A program for simulating rotational, vibrational and electronic spectra.* Journal of Quantitative Spectroscopy and Radiative Transfer, 2017. **186**: p. 221-242.
34. Niu, M.L., et al., *High resolution spectroscopy and perturbation analysis of the CO $A^1\Pi$–$X^1\Sigma^+$ (0,0) and (1,0) bands.* Molecular Physics, 2013. **111**(14-15): p. 2163-2174.
35. Field, R.W., et al., *Analysis of perturbations in the $a^3\Pi$ and $a^3\Pi$ states of CO.* Journal of Molecular Spectroscopy, 1972. **44**(2): p. 383-399.
36. Le Floch, A.C. and C. Amiot, *Fourier transform spectroscopy of the CO Ångström bands.* Chemical Physics, 1985. **97**(2): p. 379-389.
37. Kepa, R. and M. Rytel, *The Ångstrom ($B^1\Sigma^+$ - $A^1\Pi$) system of the CO molecules: new observations and analyses.* Journal of Physics B: Atomic, Molecular and Optical Physics, 1993. **26**(19): p. 3355-3362.
38. Bruggeman, P.J., F. Iza, and R. Brandenburg, *Foundations of atmospheric pressure non-equilibrium plasmas.* Plasma Sources Science and Technology, 2017. **26**(12): p. 123002.
39. Bongers, W., et al., *Plasma-driven dissociation of CO2 for fuel synthesis.* Plasma Processes and Polymers, 2017. **14**(6): p. 1600126.
40. Carbone, E., et al., *Spatio-temporal dynamics of a pulsed microwave argon plasma: ignition and afterglow.* Plasma Sources Science and Technology, 2014. **24**(1): p. 015015.
41. Fridman, A. and L.A. Kennedy, *Plasma Physics and Engineering*. ed. 2004, Boca Raton: CRC Press.
42. Moisan, M. and P. Leprince, *Experimental Evidence of Parametric Instabilities in an Unmagnetized Plasma Subjected to a Strong H.F. Electric Field.* Beiträge aus der Plasmaphysik, 1975. **15**(3): p. 83-104.
43. Lieberman, M.A. and A.J. Lichtenberg, *Principles of plasma discharges and materials processing*. 2nd ed. 2005, Hoboken, N.J.: Wiley-Interscience. xxxv, 757 p.